Production Engineering (2023) 17:511–520
https://doi.org/10.1007/s11740-022-01180-5

PROCESSES

Automated process planning in milling of hybrid components

Berend Denkena[1] · Marcel Wichmann[1] · Klaas Maximilian Heide[1] · Frederik Wiesener[1] · Hai Nam Nguyen[1]

Received: 2 September 2022 / Accepted: 15 December 2022 / Published online: 10 January 2023

Abstract
Hybrid material composites can meet the increasing demands for high strength and low weight due to their different workpiece properties. Usually, hybrid components require post-machining after their fabrication. Due to the different material properties, new challenges arise in the machining process. It is essential to recognize the course of the material boundary in order to adapt the process planning accordingly and to enable a uniform material transition during machining. This paper presents a method for automated material recognition and automatic adaptation of the process parameters considering a uniform force level during the milling of hybrid materials. This way, the load on the milling tool in the material transition area can be reduced by up to 71%, which prevents premature tool failure. An optical laser line scanner is used to localize of material transitions within hybrid components. This enables a digital mapping of the material distribution in the discretized workpiece model. In combination with an empirical force model, it is possible to predict the cutting forces of the different materials and determine the material transition area for adapting them to specified target values.

Keywords Automation · In-process measurement · Machining · Material removal · Simulation · Optimization

1 Introduction

One of the most effective methods to reduce CO_2 emissions is the mass reduction of components which results in the reduction of fuel consumption in the mobility sector [1]. Combining different materials in hybrid workpieces is a possible approach to reduce the weight of highly stressed components. By using the most qualified materials, this approach has the potential to adjust components to the local load. In the Collaborative Research Center (CRC) 1153, research is being carried out on a new type of process chain to manufacture hybrid components called Tailored Forming. By combining different materials within a component, advantages such as weight and cost reductions can be achieved with the same or improved levels of performance [2].

One current challenge in this innovative process chain is the process planning of machining. Post-machining is generally necessary to finish the workpiece geometry after the forming process, especially for functional surfaces. The use of hybrid material combinations in a workpiece results in different material-specific cutting conditions in the machining process [3]. This presents new challenges for process reliability in the machining of hybrid materials due to the different material properties, chemical composition, and transitions. It is known that the process parameters, cutting tools, and machining strategies have to be selected individually for the material and the existing microstructure to achieve a high workpiece quality [4]. Unsuitable process parameters lead to poor chip formation, long process times, and high cutting forces, which can cause tool breakage and machine damage. Further, surface quality and tool wear are coupled to the cutting forces [5]. Since machining hybrid components involve changing loads on the tool due to the material transition within the workpiece, maintaining constant cutting forces along the tool path is not possible without adapting the process parameters [6]. Different approaches for adapting the process parameters in milling regarding the cutting force are shown in [7, 8]. Accordingly, adapted machining strategies are necessary for achieving a constant workpiece and process quality.

The position and properties of the transition areas vary with workpiece shape, joining and forming method, heat treatment, and process parameters, which results in semi-finished products that are individual [9]. Denkena et al. use a

✉ Hai Nam Nguyen
nguyen@ifw.uni-hannover.de

[1] Institute of Production Engineering and Machine Tools, Leibniz Universität Hannover, An der Universität 2, 30823 Garbsen, Germany

sensor-based identification of material-specific cutting forces in turning hybrid shafts [3]. Machine data and external sensors allow the online detection of deviations in the cutting force to classify the materials. This enables material-specific process parameter adaptation and closed-loop process control. However, the process is limited by the response time of the sensors and the control system. In addition, the process parameters are not adapted until the material transition is exceeded. In roughing processes with high feed rates, this can cause damage to the milling tool and reduce the surface quality of the workpiece.

In contrast to process control, process planning can manage the adaptation in a defined transition area in advance if the initial state of the workpiece is considered. For the machining of complex components, complicated multi-axis path planning and tool path planning is also necessary [10]. Individual planning of processes under consideration of changing boundary conditions is the goal. In this case, models are used to enable predictions. Through the simulation of machining processes, suitable process parameters can be determined and optimized [11]. Depending on the machining process, it is important to recognize the material boundary profile so that the machining can be considered accordingly in process planning on a material-specific basis.

Non-contact optical sensors are used for process planning to consider the real geometry and shape deviations of the workpiece during machining [12, 13]. The advantages of optical sensors are fast and accurate surface measurements. The detection of the workpiece itself can be achieved by contact and non-contact measuring devices [14]. Laser scanning systems are used to measure freeform surfaces and can be integrated directly into the measuring chain [15]. Similarly, Denkena et al. describe an approach for an automatic re-contouring of repair-welded tool shapes using a laser line scanner for the optical acquisition of the actual workpiece geometry [16]. The cutting force is simulated and adapted using an expanded Kienzle force model [17] combined with the multi-dexel-based material removal simulation IFW CutS [18]. Additional information can be stored in the dexel endpoints using dexel extenders, which enable the consideration of workpiece properties in process simulation.

Models for the prediction of cutting forces range from empirical formulations [17, 19], analytical approaches [20, 21], to nonlinear finite element methods [22, 23]. For the calculation of five-axis milling processes with complex engagement conditions, different empirical and analytical force models have proven to be suitable, where the cutting force is estimated from the extracted volume [6].

This paper focuses on setting suitable process parameters for machining hybrid workpieces based on a machine-integrated detection of the material transition. Using optical measurement technology, areas to be machined are localized and classified. This material classification is stored as additional information in the digital workpiece of the material removal simulation and used for automated process planning. For optimization, the expected cutting force is used as the target value to keep it within the specified ranges for the different materials.

2 Cutting force modeling

To enable precise cutting force prediction and process optimisation with stable cutting forces in milling hybrid components, an empirical force model is parameterised for steel and aluminium workpieces. To parameterize the force model, a full-factorial experimental plan is set up in which the parameters feed per tooth and depth of cut are varied. After that, experimental milling tests are carried out. In the full-factorial experiments, the depth of cut a_p is varied in six levels (0.2 mm, 0.5 mm, 0.8 mm, 1 mm, 2 mm, and 3 mm). Further, different values for the feed per tooth f_z are set (0.005 mm, 0.01 mm, 0.03 mm, 0.06 mm, 0.08 mm, and 0.1 mm). The cutting speed v_c is set to the constant value of 70 m/min for steel and 350 m/min for aluminium, according to the milling tool specifications. Machining is performed without cooling lubricant. The process forces are recorded simultaneously to the milling process and determined in a 3-axis full-cut operation for each material. A DMG Mori HSC 55 linear CNC machine was selected as CNC machine tool. 2-edged solid carbide end mills with TiN/TiAlN-coating and a diameter of 10 mm are used for the experiments. The tool length and radius are measured with a tool pre-set-up system (Zoller Venturion 450). Based on the recorded process force with a dynamometer (Kistler 9257B), the maximum cutting force F_c for both cutting edges is determined. By averaging the cutting force of both cutting edges, the effects of radial run-out error and process dynamics are compensated within the force model parameterisation and evaluations. The width of flank wear land V_B is checked regularly every 5 tests using a Keyence digital microscope VHX-600. If $V_B = 80$ µm is exceeded, a tool change is carried out to minimize the influence of tool wear in force evaluation and prediction. The workpiece materials used for the experiments are steel 20MnCr5 (AISI 5120) and aluminium AlSi1MgMn. The material properties are shown in Table 1.

Table 1 Material properties of 20MnCr5 and AlSi1MgMn

	20MnCr5	AlSi1MgMn
Density [g/cm^3]	7.75	2.70
Hardness [HB]	255	95
Tensile strength [MPa]	980–1280	310
Young's modulus [GPa]	210	70

The following force modelling based on a specific Kienzle [16] cutting force model is presented. The specific cutting force k_c can be determined with Eq. (1).

$$k_c = \frac{F_c}{b \cdot h} = k_{c1.1} \cdot \left(\frac{h}{h_0}\right)^{-m_c} \quad (1)$$

The Kienzle force model is used for the end milling of steel and aluminum. Figure 1 shows the feed per tooth (equal to maximal undeformed chip thickness for full slot milling) over the average values of the specific cutting force determined from the experiments. In Fig. 1 this is exemplarily shown for the process parameter combination $a_p = 1$ mm, $v_c = 70$ m/min and $f_z = 0.005$—0.1 mm with a R^2 of 0.987.

To increase the accuracy of the model, the regression is performed individually for each depth of cut a_p. This results in individual parameters of the force model for different depths of cut. With an average $R^2 = 0.98$, the models show a high quality for aluminum and steel. For a force prediction of an unknown cutting depth, linear interpolation or the closest value can be applied. An overview of the determined parameters and the prediction quality over the different cutting depths is given in Table 2.

3 Scanning for material detection

The laser triangulation method is used for the optical detection of the hybrid components and the transition area. The LJ-V7080 laser line scanner from Keyence [24] is integrated into the CNC milling machine tool and has already been used for geometric component detection [16]. The material

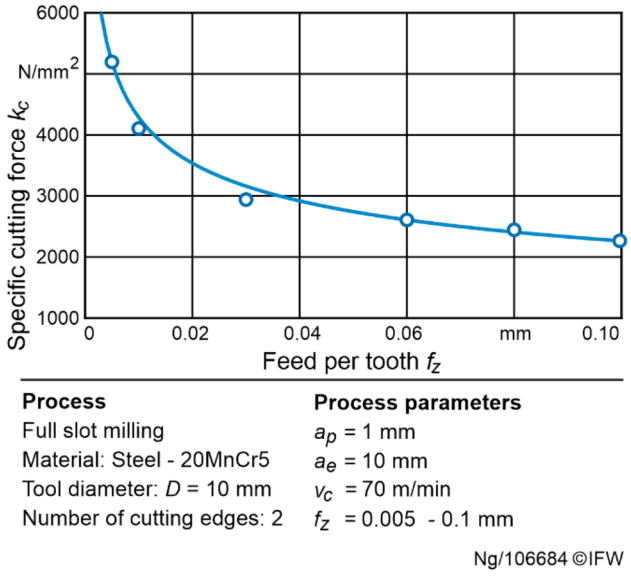

Fig. 1 Specific cutting force over feed per tooth

Table 2 Results of the cutting force model

Material	a_p [mm]	$k_{c1.1}$ [N/mm²]	m_c	R^2
AlSi1Mg-Mn	0.2	473.84	0.3980	0.984
	0.5	313.45	0.4727	0.989
	0.8	412.48	0.3891	0.996
	1.0	422.00	0.3846	0.982
	2.0	456.96	0.3429	0.992
	3.0	541.47	0.3036	0.956
Mean R^2				**0.983**
20MnCr5	0.2	1342.48	0.2690	0.997
	0.5	1289.50	0.2549	0.999
	0.8	1167.57	0.2719	0.986
	1.0	1280.16	0.2670	0.988
	2.0	1149.54	0.2690	0.971
	3.0	926.87	0.3044	0.965
Mean R^2				**0.984**

boundary of the workpieces is aligned perpendicular to the line of the laser. The laser scanner is then moved along the transition area of the two different materials. The scanning frequency is 1 kHz for all experiments. One measurement line consists of 800 points at a fixed distance of 0.05 mm. The distance of the lines is set to 1 mm. The feed rate is set to 50 mm/min for all experiments, at which the sensor moves over the samples.

In the first experimental series, different parameters of the sensor are varied using the one-factor method in two to three steps each (see Table 3). The aim is to determine the relevant parameters that have the greatest influence on the differentiation between the two selected materials. The variation of the different measurement parameters is done for one parameter at a time, while the other parameters remain at their respective default values. This results in 15 tests per sample. Both unmachined and machined workpieces are scanned. The latter are optically similar due to the lack of a soot layer in the steel and are thus a further challenge for the measuring system.

Major differences were found in the sensitivity of the parameters, laser intensity, and receiver sensitivity. The

Table 3 Investigated measurement settings

Parameter	Settings
Sensitivity	1; 3; 5
Exposure time	30 µs; 960 µs; 1920 µs
Top choice	Remove x multireflexion; remove y multi-reflexion
Receiver sensitivity	High precision; high dynamic range 3
Recording mode	Synthesis; Optimized light Intensity
Laser intensity	1–2; 50–51; 98–99

distinction in the point clouds can be seen at low sensitivity in Fig. 2. In the aluminum region, the light emitted by the sensor is reflected stronger than for steel. In the scan data, this is evident from the higher point density with aluminum. In contrast, the steel area is hardly represented in the point cloud. This makes it possible to distinguish between aluminium and steel.

In the second step, the influence of the parameters sensitivity, exposure time, and laser intensity is investigated in more detail by carrying out the experiments fully factorially at two levels in each case (see Table 4). The aim is to determine the optimum combination of settings for flat and curved surfaces. The receiver sensitivity is set to "High Precision" since better results were obtained with this setting. The other parameters were set to their default values. Additionally, the exposure time was included in the further investigation. Moreover, its range between lowest and highest value was increased because this interacts with the laser intensity. This results in 8 experiments per sample.

The workpieces are milled within one process step in this test series by bolting both components together and performing a face milling process. This eliminates disparities in different surface finishes and height differences. In addition, the scans are performed on curved workpieces to investigate the influence of the angle between the sensor and the workpiece surface. Therefore, a friction-welded shaft made of aluminum and steel with a uniformly machined surface is used (Fig. 3). The best results for the flat workpiece can be obtained with high sensitivity, low laser intensity, and long exposure time. Like in the pre-experiments, measuring points are detected on aluminum, while few points can be seen on steel. For the round shaft, the best differentiation is seen with low sensitivity and high laser intensity. With a short exposure time, steel is more difficult to recognize. At a long exposure time, both materials can be seen, with the aluminum being noisier. The angle and distance of the laser to the surface are also relevant influencing variables. Major differences are found at the edge of the shaft. However, due to the linear movement of the machine axes, the distance of the sensor to the measured surface has also increased here.

Overall, parameter combinations of the scanner can be determined that generate satisfactory measurement results to differentiate between steel and alumium.

Table 4 Measurement settings for full-factorial variation

Parameter	Settings
Sensitivity	1; 5
Exposure time	30 µs; 5000 µs
Laser intensity	1–2; 98–99

4 Process planning of hybrid workpieces

To realize a safe process adaptation, the detection of material transition areas, as well as a force model for calculating new process parameters, is required. The cutting force modeling uses the contact conditions of the milling process. These are determined using a multi-dexel-based material removal simulation, considering the respective machined material proportions. The prediction of the cutting force is used to automatically calculate and adapt suitable process parameters depending on the material to be machined as part of process planning.

4.1 Material boundary detection

The scan data from the laser line scanner contains information on the surface of the hybrid workpiece in form of point clouds. The different point densities can be used to

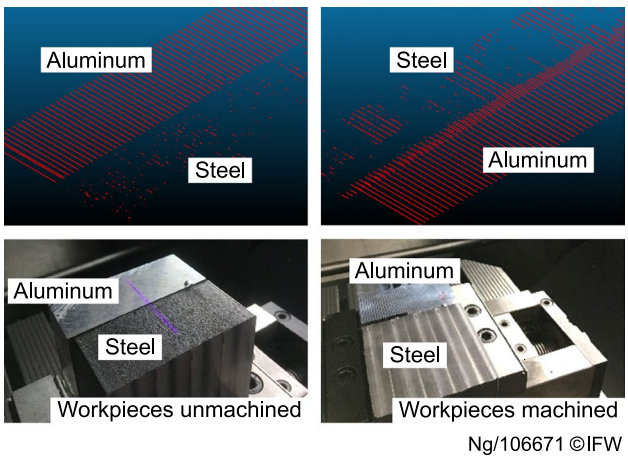

Fig. 2 Material distinction with the scan setting low sensitivity

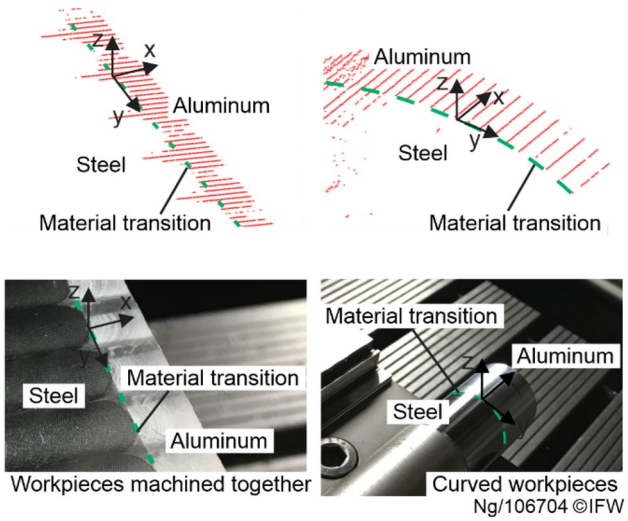

Fig. 3 Material identification for flat and curved workpieces

distinguish between steel and aluminum. To consider the real material transition in process planning, the measurement data is imported and transferred to a binary image. Starting from the original point cloud, all points are rasterized along a defined grid. The grid structure results from the point and line distance of the scan data. Image processing functions are used to allocate the material transition area. Afterward, this information is transferred to the material removal simulation (see Fig. 4).

To detect the material boundary, methods of industrial image processing are applied to the binary image. The Accord.NET library is used for this purpose (see Fig. 5). With the help of the image processing functions opening and closing (2), small imperfections in the image can be closed, and local point clusters can be removed. Image convolution with a special convolution matrix leads to an edge at the material transition. The convolution matrix is a Prewitt filter mask in the vertical orientation, which is frequently used in image processing (3). The Blob Filtering (4) ensures greater robustness in the material boundary detection by removing larger defects in the binary image. The resulting detected material boundary can be seen in red (5).

Since all actual location information is lost due to the gridding, the positions of the pixels representing the material boundary do not correspond to those in the workpiece coordinate system. Therefore, a back transformation of the pixels into the original grid is performed. Furthermore, the points are transferred to the original workpiece coordinate system via a coordinate transformation. The last step is the parameterization of the detected points representing the material

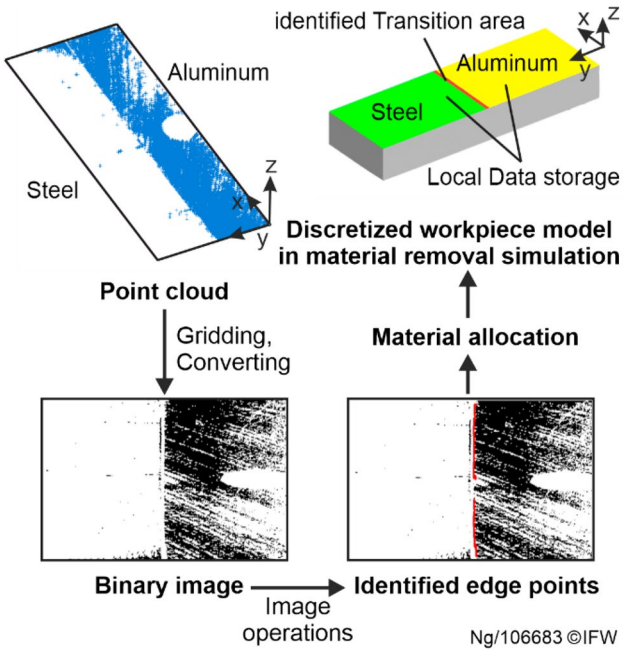

Fig. 4 Using the scanning information for the simulation

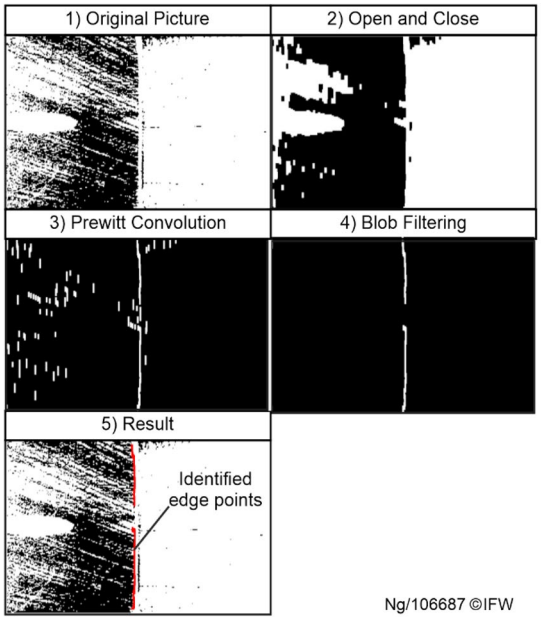

Fig. 5 Image processing operations

boundary. Based on all of these points, the gradient and the y-axis intercept of a corresponding linear function are determined. Finally, the material is divided into aluminum and steel. The assignment is made based on the point densities in the respective area.

4.2 Simulation of the cutting process of hybrid workpieces

With the help of the parameterized material boundary, the material areas are stored in the workpiece model. The material removal simulation IFW CutS is used for this purpose. This simulation platform for the technology-oriented simulation of manufacturing processes offers the basic functions of a dexel-based geometric process simulation using NC tool paths [18]. The tool movement can be simulated with very high accuracy so that the tool rotation can be reproduced within a few degrees. The overall workflow is shown in Fig. 6. The software has a modular design and is structured in different classes. The central class, which controls and links all processes, is the main controller. This takes over the communication of the plugin with the IFW CutS Kernel. In addition, different inputs and outputs are processed and passed on. At the beginning of the simulation process, the material boundary detector class locates the material boundary of the hybrid component based on the scan data. By using the dexel extenders, the material classes can be stored in the workpiece model. In this way, a clear local assignment of material areas is possible.

Tool movements, as well as the calculation of undeformed chip parameters during the simulation, are handled

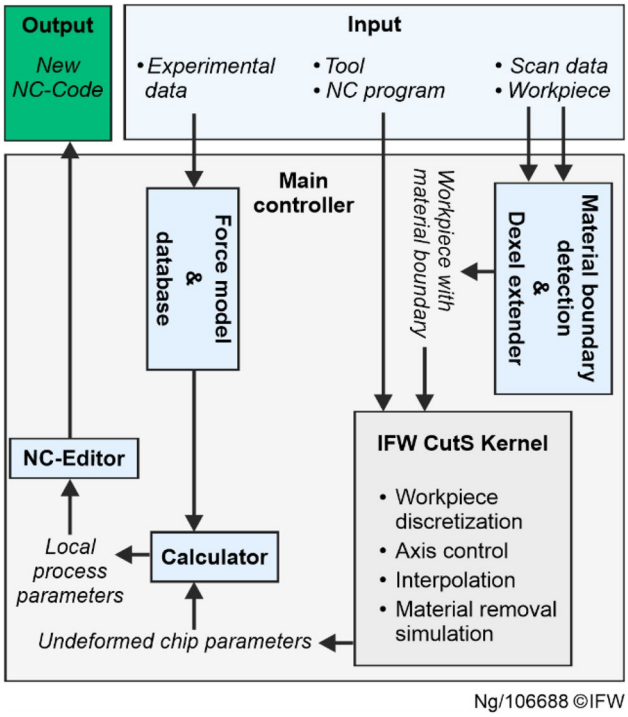

Fig. 6 Simulation workflow

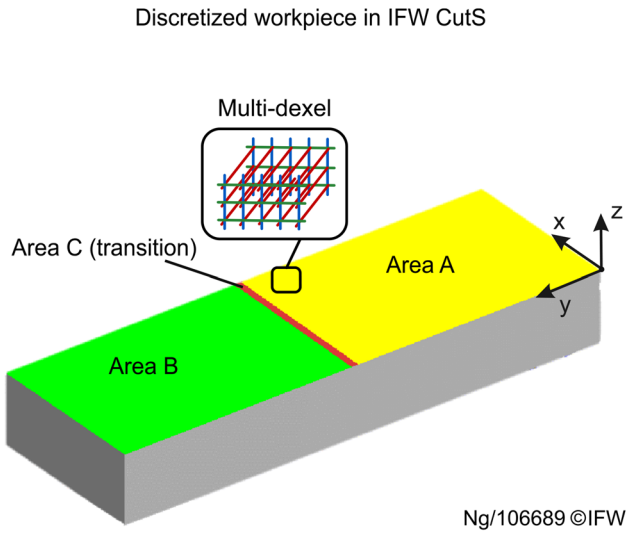

Fig. 7 Representation of the workpiece in the material removal simulation

in the IFW CutS Kernel. The calculator class includes the force model and the created database. Based on the undeformed chip parameters provided during simulation, this module calculates the process forces and derives new feed rates by rearranging the Kienzle equation for realizing specific target forces. Finally, the NC Editor class takes over the adaptation of the NC program. The calculated feed rates are inserted into the corresponding lines of the NC program together with the tool position data. Furthermore, the process parameters are adapted in the interpolators of the IFW CutS Kernel so that the changes are not only applied in the NC program but also in the simulation.

This enables the determination of cutting conditions during the machining process. In addition, the different materials can be considered during process planning. The information can be stored in the individual dexel extenders. In this case, each dexel is extended by its corresponding material class. The extenders are used here to locally assign the material class to each point based on the scan data. The proportion of the cut material can be determined in each simulation step. This will be used in the force model and allows the consideration of material-specific characteristic values ($k_{c1.1}$ and m_c) for the force prediction.

Figure 7 shows a workpiece model discretized in IFW CutS. The material classes were assigned to the dexels based on the previously determined material boundary. Differentiation is possible by coloring. A distinction is made between classes A, B, and C. While classes A and B are reserved for steel or aluminum, class C is declared a special case of the transition area. This opens the possibility of an adapted process force calculation within material transitions. Another possibility is the use of the transition area as a safe distance to the detected material boundary. In this way, the adaptation of process manipulated variables can be carried out before a material change occurs. The size of the transition area can be freely scaled by the user and influences the response time of the process parameter adaption. For high feed rates, a size of up to 4 mm is recommended. Furthermore, the heat-affected zone from the welding process can be considered via this parameter.

To determine the material removal, the workpiece must first be discretized. Besides, a model of the machine kinematics including the milling tool must be created. The simulation cycle consists of three operations: The movement of the tool based on the NC-Code, the material removal between the tool and workpiece, and the calculation of the undeformed chip parameters. During the material removal, an additional check is made to determine which type of dexels are cut by the tool. This way, the different material characteristics can be taken into account. For the calculation of the actual process forces, the depth of cut a_p and the undeformed chip thickness h are used, which can be derived from the cross-section of the undeformed chip of the simulation. Based on the force model, the corresponding values of the specific cutting force k_c are determined. This is done for aluminum (A) as well as for steel (B) (see Eqs. (2) and (3)).

$$k_{cA} = k_{c1.1A} \cdot h^{-m_{cA}} \tag{2}$$

$$k_{cB} = k_{c1.1B} \cdot h^{-m_{cB}} \tag{3}$$

The specific cutting force k_c used for the force calculation results from the proportion-dependent combination of the variables k_{cA} and k_{cB}. The percentage of the cut dexels of aluminum X_A and steel X_B is determined in each case via the dexel extenders. The specific cutting force k_c changes according to the material cut according to Eq. (4). The determination of the current k_c value based on the cutting proportions calculated via the dexel extenders thus enables precise cutting force calculation, regardless of the complexity of the material transition.

$$k_c = X_A \cdot k_{cA} + X_B \cdot k_{cB} \tag{4}$$

The cutting force F_c can be calculated according to Eq. (5).

$$F_c = b \cdot h \cdot k_c \tag{5}$$

The modeled forces are used to adapt the process parameters. The calculation of new process parameters to achieve a target force in both materials is similar to the calculation of the process forces. The target undeformed chip thickness h_{Target} is calculated by rearranging Kienzle's Eq. (6). It is then converted into the target feed rate for the NC-Code based on the current cross-section of the undeformed chip.

$$h_{Target} = \left(\frac{F_{cTarget}}{k_{c1.1} \cdot b} \right)^{\frac{1}{1-m_c}} \tag{6}$$

The newly calculated process parameters are stored in the memory with the current tool position. Based on this, the NC program is adapted, and the axis interpolators are updated. Since an adaptation of the process parameters with each rotation is practically not feasible, an interval size between 0.1 and 0.5 mm is recommended for the adaptation.

The accuracy of the simulation results depends on the resolution of the discretized workpiece on the one hand and on the choice of the time step on the other hand. Both can be specified before the simulation start. A dexel density of 60 dexels per mm in each spatial direction proves to be an acceptable compromise between computation time and accuracy. The time step is computed dynamically depending on the spindle speed so that a defined degree resolution of the tool rotation is achieved. A degree resolution in 5° steps provides satisfactory results.

5 Validation on hybrid workpieces

To investigate and evaluate the overall method of process parameter adaptation, 20 validation experiments are carried out. Target values for the cutting force and the depth of cut are varied in different scenarios at real material transitions. The target force ranges from 40 to 300 N, while the depth of cut is varied from 0.9 mm to 3.0 mm. The feed rate is adjusted by the system according to the presented approach. Further, the cutting speed v_c is adapted automatically according to the material based on the manufacturer's specifications. Thus, $v_c = 70$ m/min for steel and $v_c = 350$ m/min are used for aluminum as in the previous experiments. Milling was performed on two blocks of steel and aluminum bolted together so that material changes occur during the process. In addition, 8 further milling tests were performed on a friction-welded hybrid shaft. In contrast to the hybrid shaft, the aluminum and steel blocks have a gap between the materials because they were not welded. Figure 8 shows images of the transition areas at 50-fold magnification. The gap between the aluminum and steel blocks is 153 µm. A seamless transition can be observed for the hybrid shaft.

All milling scenarios and the relative model deviation for each material are shown in Table 5. The models show high deviations if the determined f_z reaches extremely low or high values outside the test range of the experimental data. Especially for low target cutting forces, this can be observed. For the validation tests, the average relative model deviation is 9.1% for the hybrid blocks (5.5% for the aluminum model and 12.7% for the steel model). For the hybrid shafts, the average relative model deviation is 11.1% (16.9% for the aluminum model and 5.2% for the steel model).

The effect of adapting the milling process during the transition from aluminum to steel on the cutting force is shown in Fig. 9. The maxima of the force component F_x in the workpiece coordinate system correspond to the cutting force F_c on the tool. A balancing of the forces and a uniform force

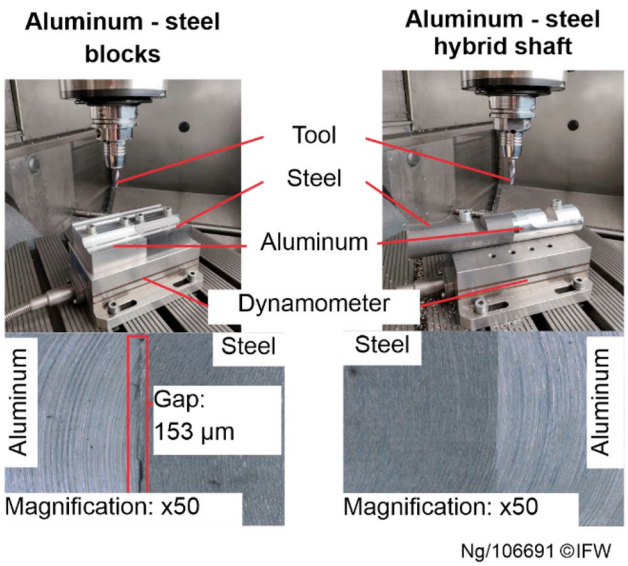

Fig. 8 Experimental setup: Validation milling experiments

Table 5 Validation experiments

a_p [mm]	Target force [N]	Deviation aluminium [%]	Deviation steel [%]
Hybrid blocks: Cutting direction: aluminum to steel			
0.9	40	4.16	34.07
0.9	80	4.90	20.27
1.6	80	0.67	23.52
1.2	120	0.04	4.57
1.2	160	4.40	4.78
2.0	160	0.78	10.93
2.0	200	0.44	8.51
3.0	250	0.08	14.53
2.0	300	0.69	6.91
Hybrid blocks: Cutting direction: steel to aluminum			
0.6	40	6.62	27.30
1.2	40	9.44	18.58
1.2	80	2.51	9,83
0.9	120	10.07	13.80
1.6	120	4.68	4.97
1.6	160	5.61	1.93
1.6	200	23.95	20.40
3.0	200	7.84	3.64
2.0	250	6.59	3.06
1.6	300	12.29	19.56
3.0	300	4.39	2.04
Hybrid shafts: Cutting direction: aluminum to steel			
1.2	80	4.47	8.00
1.2	120	23.59	0.70
1.2	160	23.15	2.72
1.6	200	29.90	7.65
Hybrid shafts: Cutting direction: steel to aluminum			
1.2	80	14.13	12.26
1.2	120	10.34	2.61
1.2	160	12.17	1.55
1.6	200	17.76	6.23

transition can thus be ensured. When adapting, a reduction in force can be seen in aluminum near the transition to steel. This follows from the user-defined safety zone, where the feed rate is already reduced before entering steel. In comparison to the original process parameters, the validation tests show a force reduction up to 70.5% at the transition area by process adaption.

The root mean square error (RMSE) between the target cutting forces and the measured forces is 17.79 N for the machining of the aluminum-steel blocks. This is the average value for both materials. For the machining of the friction-welded hybrid shaft, the RMSE is 29.97 N which is almost twice as large as the aluminum-steel blocks. In this case, a particularly strong deviation of the model is observed in the aluminum material. One possible reason is the thermal effect caused by the friction welding process and an associated change in the material structure, resulting in a slight change in the machinability of the aluminum material. The force measurements indicate this, with a uniform reduction in the process force over about three seconds before the transition from aluminum to steel in the hybrid shaft. To confirm this hypothesis further investigations are necessary.

6 Conclusion and outlook

This paper presents a force model for predicting the cutting force of milling hybrid workpieces with different materials. Based on this and a machine-integrated detection of the material transition, the process parameters are adapted

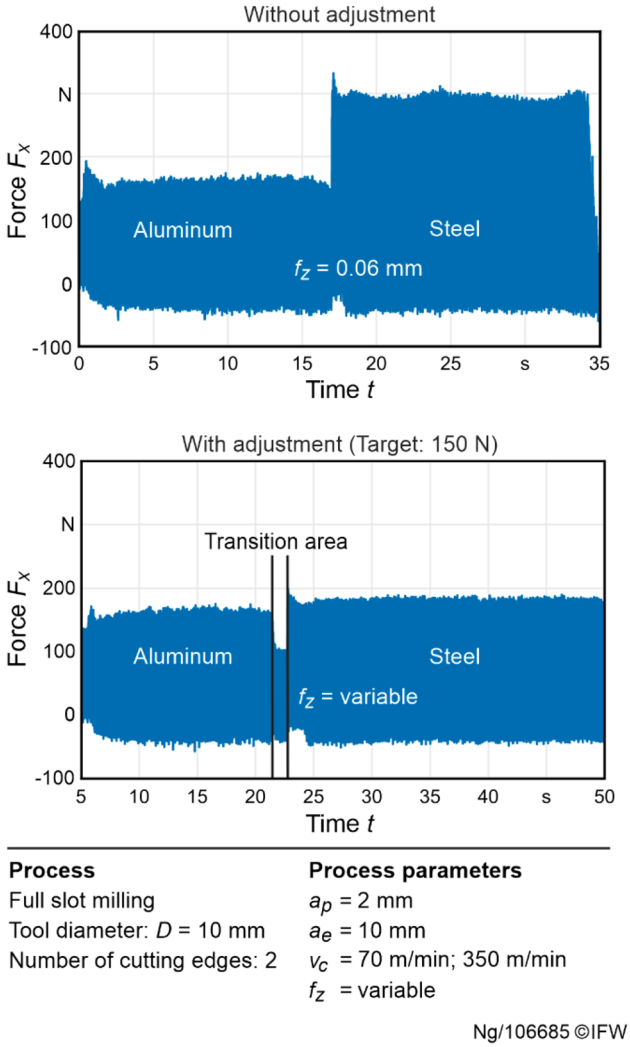

Fig. 9 Validation experiments with the hybrid block

for a uniform transition. This leads to a force reduction of up to 70.5% in the transition area and a balanced end mill load. By allocating and storing the material locally on the workpiece as additional information, different proportions of the material can be considered in the material removal simulation. With this extended determination of the local cutting conditions, the cutting forces can be predicted for different materials in the milling process of hybrid workpieces. The relative model deviation is 9.1% on average for setting target forces for the hybrid blocks and 11.1% for the hybrid shafts.

In future work, the adaption in the transition zone of the material will be further investigated. Additional research is necessary for defining the size of the safety zone to determine the actual start of the process parameter adaptation depending on the detected material transition. Especially for more complex workpiece geometries, this aspect is essential.

Acknowledgements The results presented in this paper were obtained within the Collaborative Research Center 1153 "Process chain to produce hybrid high performance components by Tailored Forming". The authors would like to thank the German Research Foundation (DFG) for the financial and organisational support of this project.

Funding Open Access funding enabled and organized by Projekt DEAL.

Data availability The datasets generated and analyzed during the current study are available from the corresponding author on reasonable request.

References

1. Goede M, Stehlin M, Rafflenbeul L, Kopp G, Beeh E (2009) Super Light Car—lightweight construction thanks to a multi-material design and function integration. Eur Transp Res Rev 1(1):5–10
2. Behrens B-A, Chugreev A, Matthias T (2018) Characterisation of the joining zone of serially arranged hybrid semi-finished components. In: Proceedings of the 21st international Esaform conference on material forming: Esaform 2018, Palermo, Italy. 23–25 April 2018. Author(s), p. 40002.
3. Denkena B, Bergmann B, Breidenstein B, Prasanthan V, Witt M (2019) Analysis of potentials to improve the machining of hybrid workpieces. Prod Eng Res Devel 13(1):11–19
4. Byrne G, Dornfeld D, Denkena B (2003) Advancing cutting technology. CIRP Ann 52(2):483–507
5. Jayaram S, Kapoor SG, DeVor RE (2001) Estimation of the specific cutting pressures for mechanistic cutting force models. Int J Mach Tools Manuf 41(2):265–281
6. Karunakaran KP, Shringi R, Ramamurthi D, Hariharan C (2010) Octree-based NC simulation system for optimization of feed rate in milling using instantaneous force model. Int J Adv Manuf Technol 46(5–8):465–490
7. Shimada T, Nakamoto K, Shirase K (2010) Machining strategy to adapt cutting conditions under digital copy milling concept. JAMDSM 4(5):924–935
8. Tandon V, El-Mounayri H, Kishawy H (2002) NC end milling optimization using evolutionary computation. Int J Mach Tools Manuf 42(5):595–605
9. Herbst S, Maier HJ, Nürnberger F (2018) Strategies for the heat treatment of steel-aluminium hybrid components. HTM 73(5):268–282
10. Liang F, Kang C, Fang F (2021) A review on tool orientation planning in multi-axis machining. Int J Prod Res 59(18):5690–5720
11. Altintas Y, Kersting P, Biermann D, Budak E, Denkena B, Lazoglu I (2014) Virtual process systems for part machining operations. CIRP Ann 63(2):585–605

12. Azzam N, Chaves-Jacob J, Boukebbab S, Linares J-M (2014) Adaptation of machining toolpath to distorted geometries: application to remove a constant thickness on rough casting prosthesis. Int J Adv Manuf Technol 72(5–8):1073–1083
13. Kuss A, Drust M, Verl A (2016) Detection of workpiece shape deviations for tool path adaptation in robotic deburring systems. Procedia CIRP 57:545–550
14. Jeon H, Lee J, Yang J (2016) A touch-probe path generation method through similarity analysis between the feature vectors in new and old models. J Mech Sci Technol 30(10):4705–4716
15. Son S, Park H, Lee KH (2002) Automated laser scanning system for reverse engineering and inspection. Int J Mach Tools Manuf 42(8):889–897
16. Denkena B, Dittrich M-A, Heide KM (2019) Automatic re-contouring of repair-welded tool moulds. Procedia Manuf 40:45–50
17. Kienzle O (1952) Die bestimmung von kräften und Leistungen an spanenden Werkzeugen und Werkzeugmaschinen. VDI-Z 94(11):299–305
18. Denkena B, Böß V (2009) Technological NC simulation for grinding and cutting processes using CutS. In: Proceedings of the 12th CIRP Conference on Modelling of Machining Operations. May 7–8, 2009, Donostia-San Sebastián, Spain. May 7–8. Mondragon Unibertsitateko, Arrasate-Mondragón, Gipuzkoa, pp. 563–566.
19. Newby G, Venkatachalam S, Liang SY (2007) Empirical analysis of cutting force constants in micro-end-milling operations. J Mater Process Technol 192–193(1):41–47
20. Fang N, Jawahir IS (2002) Analytical predictions and experimental validation of cutting force ratio, chip thickness, and chip backflow angle in restricted contact machining using the universal slip-line model. Int J Mach Tools Manuf 42(6):681–694
21. Merchant ME (1945) Mechanics of the metal cutting process. I. Orthogonal cutting and a type 2 chip. J Appl Phys 16(5):267–275
22. Man X, Ren D, Usui S, Johnson C, Marusich TD (2012) Validation of finite element cutting force prediction for end milling. Proc CIRP 1:663–668
23. Özel T, Altan T (2000) Process simulation using finite element method—prediction of cutting forces, tool stresses and temperatures in high-speed flat end milling. Int J Mach Tools Manuf 40(5):713–738
24. Keyence (2022) Keyence Corporation: Data Sheet LJ-V7080 Sensor Head.